PROTON-PROTON AND PROTON-ANTIPROTON ELASTIC SCATTERING IN THE DUAL UNITARY SCHEME*

By J. Kalinowski

Institute of Theoretical Physics, Warsaw University**

(Received March 17, 1976)

The pp and $p\bar{p}$ elastic scattering amplitudes are calculated in the dual unitary scheme. It is shown that the crossing symmetry of the pomeron term in the low energy region is restored due to the presence of annihilation channels in the $p\bar{p}$ scattering. The total annihilation cross section and the t-dependence of the elastic scattering amplitudes are also discussed.

1. Introduction

Duality and unitarity consititute together very powerful constraints on hadron collision amplitudes. In recent years a method [1–3] was proposed for calculating the imaginary part of the elastic scattering amplitude as a shadow of the multiparticle processes,

$$2 \operatorname{Im} \langle i|T|i\rangle = \sum_n \langle n|T^*|i\rangle \langle n|T|i\rangle, \tag{1}$$

when the latter are described in the framework of a multi-Regge cluster model obeying semi-local duality and exchange degeneracy.

In the first approximation one assumes that the sum in Eq. (1) is taken only over the non-diffractive multiparticle states. Groups of particles with small invariant masses $M < \overline{M}$ are described in terms of the resonance (cluster) approximation. Semi-local duality then allows to replace the multireggeon exchange diagrams appearing in the unitarity sum by reggeon loop diagrams, as illustrated in Fig. 1. The reggeon loop can be either crossed or uncrossed corresponding to the quark diagrams (a) and (b) of Fig. 2, respectively. It has been shown [2] that the elastic scattering amplitude divides automatically into two components. One of them consists of contributions from the uncrossed reggeon loop diagrams and thus corresponds to the exchange of nonzero internal quantum numbers. The second component consists of diagrams with at least one crossed loop. It dominates

* Work supported in part by the U.S. National Science Foundation under the Grant GF-42060.

** Address: Instytut Fizyki Teoretycznej, Uniwersytet Warszawski, Hoża 69, 00-681 Warszawa, Poland.

at high energy and has vacuum t-channel quantum numbers. Consequently, it can be identified with the pomeron exchange contribution. Numerical calculations [2] were performed for the meson-meson (MM), meson-baryon (MB) and baryon-baryon (BB) scattering. It was assumed that only the leading meson exchange is important along the multiperipheral chain.

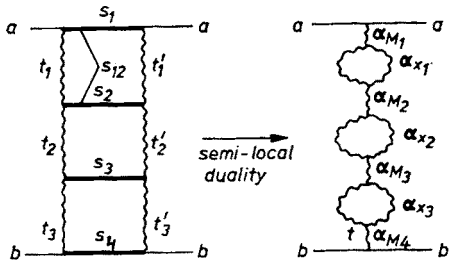

Fig. 1. a — resonance (cluster) production graph, b — reggeon loop graph

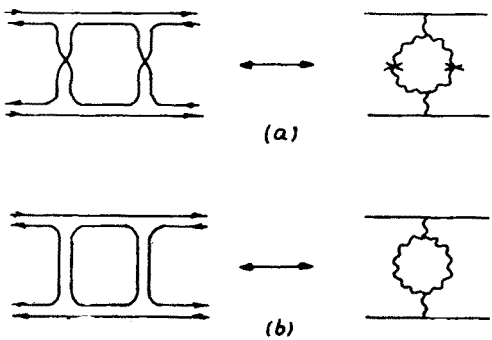

Fig. 2. The two types of allowed reggeon loops: (a) crossed loop and (b) uncrossed loop

In this paper we study BB and baryon-antibaryon ($B\bar{B}$) elastic scattering in the dual unitary scheme of Refs [1, 2]. In particular we investigate the problem of the crossing symmetry of the pomeron exchange contribution in BB and $B\bar{B}$ collisions.

One cannot obtain a crossing symmetric pomeron term within the meson exchange approximation. The problem appears already at the single loop diagram level: the diagram (a) of Fig. 2 is present in BB but not on $B\bar{B}$ scattering. Also taking into account all the higher order meson loop diagrams, we could perhaps obtain asymptotically equal, for BB and $B\bar{B}$, pomeron terms but they differ at any finite energy [4].

Eylon and Harari [5] pointed out that it might be possible to arrange a crossing symmetric pomeron if one included annihilation channels into the unitarity sum for $B\bar{B}$ scattering. The role of baryon exchange has been also stressed by Freund and Rivers [6] and Guła and Pennington [7] but in a somewhat different approach. They take exotic mesons in the intermediate state and conclude that in the low energy region the pomeron in the proton--antiproton ($p\bar{p}$) elastic scattering is given by the single baryon loop of Fig. 3 whereas in pp by the single meson loop of Fig. 2a.

We present here a more systematic calculation of the pp and $p\bar{p}$ elastic scattering amplitudes which we hope to be accurate enough in the tens GeV energy region. We have taken into account meson and baryon loops at the one and two loops level. We keep cut-off value of resonance (cluster) masses $\bar{M} = 2.45$ GeV ($\bar{M}^2 = \bar{s} = 6$ GeV^2 as in the original work [2]). It turns out that the contribution from the annihilation channels indeed restore

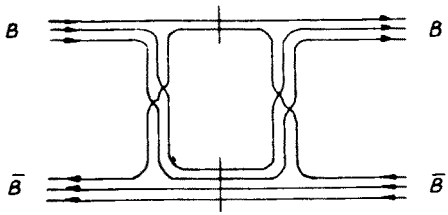

Fig. 3. Baryon loop proposed in Ref. [7]. Slashes denote intermediate states of arbitrary mass (allowed by energy conservation)

crossing symmetry of the pomeron, as suggested by Eylon and Harari. However, other meson and baryon two loop diagrams are also important in the low energy region of both reactions.

We have found that the pomeron contribution

(*i*) is equal for the pp and $p\bar{p}$ elastic scattering,

(*ii*) is approximately energy independent for $10 < s < 50$ GeV^2,

(*iii*) has a reasonable slope in t.

We have also calculated the t-dependence of the full $d\sigma_{el}/dt$ and found the slope parameters for both reactions to be of the right order of magnitude. The total $p\bar{p}$ annihilation cross section has a reasonable value as well.

The paper is organised as follows. In the next Section we discuss general assumptions and present diagram counting. Section 3 contains numerical details and discussion of our results. A summary of our results is given in the last Section.

2. The loop diagrams

We discuss now the one- and two-reggeon exchange resonance (cluster) diagrams taken into account in our calculation.

Diagrams considered by us are presented in Fig. 4. We follow the scheme of Ref. [5] and identify the graphs with no quark, two quark and four quark lines exchanged in the t-channel as the contribution to the elastic scattering amplitude of the pomeron term, meson term and exotic term, respectively.

We restrict ourselves to diagrams with resonances (clusters) in the s-channel which can be represented by two or three quark lines and neglect all exotic states ($qq\bar{q}\bar{q}$ etc.). Up to now there is no definite experimental evidence [8] for the existence of such resonances. Even if they exist, their masses are presumably larger than 2 GeV [9] and, therefore, mostly above our parameter $\bar{M}$. However, one should remember that in our approach we include high mass exotic states in the s-channel in the sense of semilocal duality. They are dual

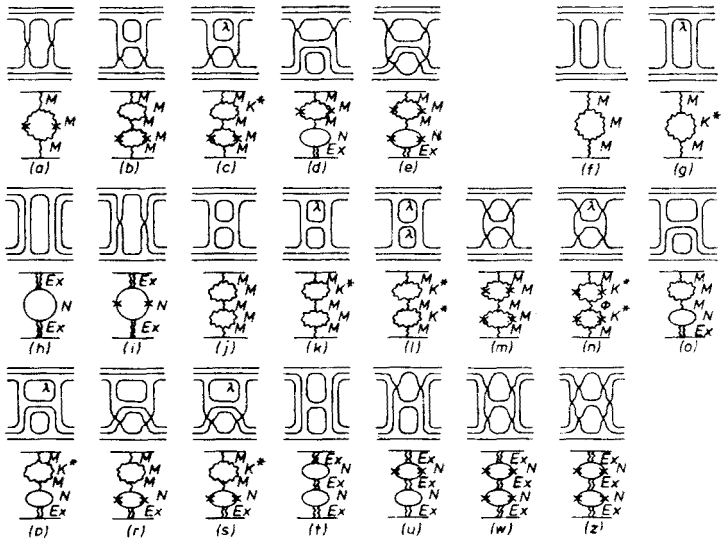

Fig. 4. Allowed quark (and loop) diagrams at the one and two loops level for the pp (a — e) and $p\bar{p}$ (f — z) elastic scattering. In the loop diagrams the wavy line, round line and double wavy line denote the meson, baryon and exotic trajectories, respectively

to the t-channel meson exchange in $B\bar{B}$ scattering and appear when we sum over the diagrams[1] shown in Fig. 5. Although, as argued above, the first diagram of the sum has been neglected by us, the two loop diagrams of Fig. 5 are included in our calculation.

It follows from the exchange degeneracy of the meson trajectories that diagrams involving twists in the produced lines (Fig. 6a) or both crossed and uncrossed Regge exchanges in the same loop (Fig. 6b) are absent.

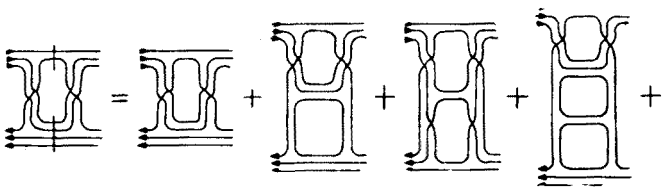

Fig. 5 .Unitarity equation for an exotic intermediate state in terms of the cluster diagrams (cluster masses satisfy the condition $M < \overline{M}$)

In our calculation we take, in the first approximation, the baryon exchange also as an exchange degenerate pair and, consequently, neglect diagrams with a baryon exchange similar to those of Fig. 6.

One can easily check that there is no one loop diagram contributing to the pomeron in the $p\bar{p}$ elastic scattering. At the two loop level there are three types of diagrams building

[1] Our diagrams always describe intermediate states whose masses satisfy the relation $M < \overline{M}$. The only exceptions are the LHS diagram of Fig. 5 and the diagram of Fig. 3 (they are marked by slashes).

the pomeron. Graphs 6 (m) and (n) of Fig. 4 are the meson loop diagrams, graphs (r) and (s) represent contributions of baryon exchange in non-annihilation channels and graph (z) represents annihilation contribution to the pomeron term. Diagrams (f), (g), (i), (j), (k), (l),

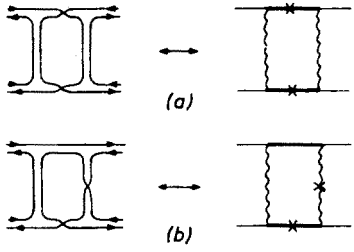

Fig. 6. Meson diagrams forbidden in our approximation

(o), (p), (u) and (w) in Fig. 4 give the meson term and graphs (h) and (t) build the exotic term. Graphs (i), (h), (t), (u), (w) and (z) of Fig. 4 generate the total pp annihilation cross section.

In the pp elastic scattering all diagrams (a — e) give the pomeron term.

3. Details and results

Now we wish to specify the analytical representation of diagrams, parameters of the exchanged trajectories and their coupling constants.

The analytic formulae for the one and two loop diagrams of Fig. 4 are given in Appendix A. They are a direct generalisation of the well-known triple-Regge formula. We take them for meson and baryon loop diagrams as well. The effective coupling constants G of all diagrams in Fig. 4 are given in Table I.

The t-dependence of the triple-Regge vertices and phase factors for loops, which constitute formulae (A1) and (A2), are explained in Appendix B. We note here that parametrization (B1) is taken also for BBM and BBEx vertices as suggested by the results of Dias de Deus and Uscherson[2] [13].

Semi-local duality for the meson trajectory-particle and the meson trajectory-meson trajectory amplitudes is well established [10]. As meson exchanges we take the meson trajectories of the vector-tensor nonet which we assume to be exchange degenerate. We distinguish three types of trajectories which describe the SU(3) symmetry breaking in the trajectory intercepts and according to their quark content

$\alpha_M = 0.5$ p, n quarks only: f, ω, ϱ, A_2,

$\alpha_{K''} = 0.35$ p or n and λ quarks: K^*, K^{**},

$\alpha_\varphi = 0.$ λ quarks only: ϕ, f',

$\alpha' = 1.\ \mathrm{GeV}^{-2}.$

[2] I am indebted to dr Dias de Deus for a discussion on this point.

TABLE I

List of parameters and coupling constants used for evaluating the diagrams of Fig. 4. We use the following abbreviations: $g_{fff} = g$, $g_{\mathrm{NNEx}} = g_{\mathrm{Ex}}$, $g_{\mathrm{NN}f} = g_{\mathrm{N}}$, $\gamma^{\mathrm{p}}_{\mathrm{Ex}} = \gamma_{\mathrm{Ex}}$, $\gamma^{\mathrm{p}}_{\mathrm{M}} = \gamma_{\mathrm{M}}$

	α_{M_1}	α_{M_2}	α_{M_3}	α_{x_1}	α_{x_2}	b_1	b_2	G
a	0.5	0.5	—	0.5	—	0	—	$(\gamma_\omega^2+\gamma_f^2)\,16g^2$
b	0.5	0.5	0.5	0.5	0.5	1	0	$(\gamma_\omega^2+\gamma_f^2)\,16g^2\,16g^2\times 2$
c	0.5	0.5	0.35	0.5	0.5	1	0	$(\gamma_f^2+\gamma_\omega^2)\,8g^2\,16g^2\times 2$
d	0.5	0.5	−1.	0.5	−0.35	0	1	$(\gamma_f+\gamma_\omega)\,16g^2\,4g_{\mathrm{N}}g_{\mathrm{Ex}}\gamma_{\mathrm{Ex}}\times 2$
e	0.5	0.5	−1.	0.5	−0.35	0	0	$(\gamma_f+\gamma_\omega)\,16g^2\,4g_{\mathrm{N}}g_{\mathrm{Ex}}\gamma_{\mathrm{Ex}}\times 2$
f	0.5	0.5	—	0.5	—	1	—	$(\gamma_f^2+\gamma_\omega^2+\gamma_\varrho^2+\gamma_A^2)\,16g^2/2$
g	0.5	0.5	—	0.35	—	1	—	$(\gamma_f^2+\gamma_\omega^2+\gamma_\varrho^2+\gamma_A^2)\,8g^2/2$
h	−1.	−1.	—	−0.35	—	1	—	$4(g_{\mathrm{Ex}}\gamma_{\mathrm{Ex}})^2$
i	−1.	−1.	—	−0.35	—	0	1	$4(g_{\mathrm{Ex}}\gamma_{\mathrm{Ex}})^2$
j	0.5	0.5	0.5	0.5	0.5	1	1	$(\gamma_f^2+\gamma_\omega^2+\gamma_\varrho^2+\gamma_A^2)\,16g^2\,16g^2$
k	0.5	0.5	0.5	0.35	0.5	1	1	$(\gamma_f^2+\gamma_\omega^2+\gamma_\varrho^2+\gamma_A^2)\,8g^2\,16g^2\times 2$
l	0.5	0.5	0.5	0.35	0.35	1	1	$(\gamma_f^2+\gamma_\omega^2+\gamma_\varrho^2+\gamma_A^2)\,8g^2\,8g^2$
m	0.5	0.5	0.5	0.5	0.5	0	0	$(\gamma_f^2+\gamma_\omega^2)\,16g^2\,16g^2$
n	0.5	0.	0.5	0.35	0.35	0	0	$(\gamma_f^2+\gamma_\omega^2)\,(8\sqrt{2}\,g^2)^2$
o	−1.	0.5	0.5	−0.35	0.5	1	1	$(\gamma_f+\gamma_\omega+\gamma_\varrho+\gamma_A)\,16g^2\,4g_{\mathrm{N}}g_{\mathrm{Ex}}\gamma_{\mathrm{Ex}}\times 2$
p	−1.	0.5	0.5	−0.35	0.35	1	1	$(\gamma_f+\gamma_\omega+\gamma_\varrho+\gamma_A)\,8g^2\,4g_{\mathrm{N}}g_{\mathrm{Ex}}\gamma_{\mathrm{Ex}}\times 2$
r	−1.	0.5	0.5	−0.35	0.5	0	1	$(\gamma_f+\gamma_\omega)\,16g^2\,4g_{\mathrm{N}}g_{\mathrm{Ex}}\gamma_{\mathrm{Ex}}\times 2$
s	−1.	0.5	0.5	−0.35	0.35	0	1	$(\gamma_f+\gamma_\omega)\,8g^2\,4g_{\mathrm{N}}g_{\mathrm{Ex}}\gamma_{\mathrm{Ex}}\times 2$
t	−1.	−1.	−1.	−0.35	−0.35	1	1	$4(\gamma_{\mathrm{Ex}}g_{\mathrm{Ex}})^2\,4g_{\mathrm{Ex}}^2$
u	−1.	−1.	−1.	−0.35	−0.35	0	1	$4(\gamma_{\mathrm{Ex}}g_{\mathrm{Ex}})^2\,4g_{\mathrm{Ex}}^2\times 2$
w	−1.	−1.	−1.	−0.35	−0.35	0	0	$4(\gamma_{\mathrm{Ex}}g_{\mathrm{Ex}})^2\,4g_{\mathrm{Ex}}^2$
z	−1.	−1.	−1.	−0.35	−0.35	0	0	$4(\gamma_{\mathrm{Ex}}g_{\mathrm{Ex}})^2\,4g_{\mathrm{Ex}}^2\times 2$

Hoyer et al. also discuss duality in $\mathrm{B\bar{B}}$ processes and they conclude that meson resonances in the baryon trajectory-antibaryon scattering are dual to an exotic trajectory with an intercept [11]

$$-0.5 \geqslant \alpha_{\mathrm{Ex}}(0) \geqslant -1.4. \tag{2}$$

Pickering [9] quotes $\alpha_{\mathrm{Ex}} = -1.3$, Pennington and Guła [7] $\alpha_{\mathrm{Ex}} = -1.2$. For our calculation we have taken

$$\alpha_{\mathrm{Ex}}(t) = -1.+t. \tag{3}$$

For baryon exchange we have a possibility of the $\Delta_\delta(\frac{3}{2}^+(1236), \frac{7}{2}^+(1924), \frac{11}{2}^+(2450)$ resonances), nucleon $\mathrm{N}_\alpha(\frac{1}{2}^+(938), \frac{5}{2}^+(1688), \frac{9}{2}^+(2220)$ resonances), nucleon $\mathrm{N}_\gamma(\frac{3}{2}^-(1512), \frac{7}{2}^-(2210), \frac{11}{2}^-(2640)$ resonances) and other lower lying trajectories. While Δ_δ has the highest intercept and should dominate at high energy its couplings are much weaker than the nucleon ones [7]. We are concerned with the low energy region and consequently we neglect the exchange of this trajectory. We take into account only nucleon trajectories N_α and N_γ assuming exchange degeneracy between them and the following parametrization:

$$\alpha_{\mathrm{B}}(u) = \alpha_{\mathrm{N}}(u) = -0.35+0.85u. \tag{4}$$

We also neglect unnatural parity exchange. It has been shown [12] that, at fixed incoming energy $\sqrt{s}$, the unnatural parity exchange becomes important when the masses of produced resonances are big. Also, the coupling of the pion loop to the external protons is smaller than the coupling of the baryon loop. We have checked that in our approach with the cut-off value $\overline{M} = 2.45$ GeV for the resonance masses the pion exchange contribution is negligible in the energy range under discussion.

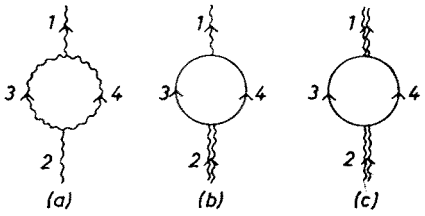

Fig. 7. Three types of loops

Finally, we must specify couplings γ_M^p, g_{fff}, g_{NNf}, g_{NNEx} and γ_{Ex}^p. From experimental data we have $\gamma_f^p = 10\ \text{GeV}^{-1}$. Other meson couplings to the external protons are given by the SU(3) symmetry. Triple f-coupling has its bootstrap value about $8\ \text{GeV}^{-1}$ [3]. We take $g_{fff} = 8\ \text{GeV}^{-1}$. From a phenomenological analysis it has been recently found [7] that

$$g_{NNEx}\gamma_{Ex}^p \approx g_{NNf}\gamma_f^p = 270\ \text{GeV}^{-2}. \tag{5}$$

Therefore, $g_{NNf} = 27\ \text{GeV}^{-1}$ and we are left with one free parameter g_{NNEx}. All the parameters used in this calculation are listed together in Table I.

Numerical calculations were performed for $10 < s < 64\ \text{GeV}^2$. Results are given in

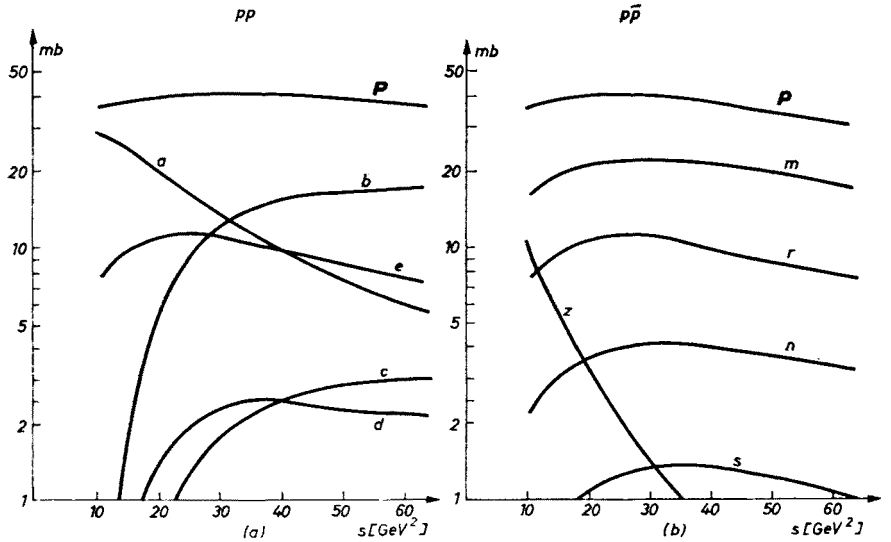

Fig. 8. Pomeron term in (a) the pp and (b) $p\bar{p}$ scattering

Fig. 8 and Fig. 9. The $\sigma_{tot}(pp)$ is almost s-independent in the range $10 < s < 60\ GeV^2$. For higher energies the cross section calculated in the two loop approximation begins to decrease.

Now we turn our attention to the pomeron term in $p\bar{p}$ scattering. Fig. 8 shows that even in the low energy region the dominant contribution comes from the diagram (m) of Fig. 4 with two crossed meson loops. Graphs 4 (r) and (s) alone are not sufficient to compensate the difference between the meson loop contribution to the pomeron terms in pp

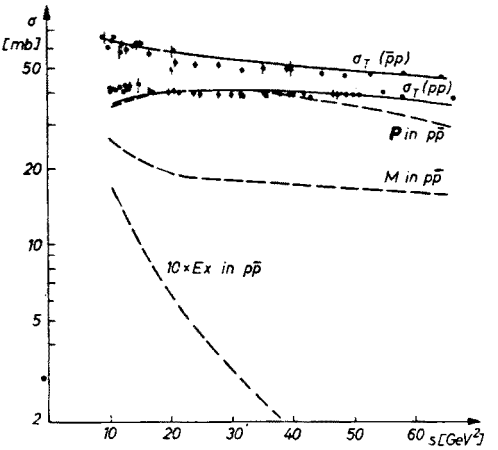

Fig. 9. The s-dependence of the calculated $\sigma_{tot}(pp)$ and $\sigma_{tot}(p\bar{p})$

and $p\bar{p}$ collisions. Moreover, when we take these graphs into account we must include diagrams 4 (d) and (e) in pp scattering. Contributions coming from both sets of graphs are equal and the pomeron terms in both channels are still different. It turns out that the "missing piece" of the pomeron in the $p\bar{p}$ scattering is given by the graph 4 (z) representing annihilation channels. When we take $g_{NNEx} = 23\ GeV^{-1}$ (a value compatible with $g_{NNEx} \approx g_{NN_f}$ as follows from the one loop dominance [13]), we obtain almost equal pomeron terms in both channels in the range $10 < s < 45\ GeV^2$. When the incoming energy grows, higher order loop diagrams become important first in the $p\bar{p}$ scattering (these with annihilation channels), than in the pp scattering (Fig. 8). This effect explains why at the two loop level **P** in $p\bar{p}$ falls, with an increase of energy, faster than **P** in pp.

Now, we have fixed all parameters and we can check whether other predictions of our scheme are reasonable.

Fig. 9 shows that the ratio $\sigma_T(pp)/\sigma_T(p\bar{p})$ is comparable with the experimental data. The output meson and exotic exchange terms in $p\bar{p}$ elastic scattering are also shown in Fig. 9. The energy dependence of these terms can be approximately fitted by powers of s, as seen in Fig. 10, which then gives us the effective output intercepts $\alpha_M^{out} \approx 0.6$ $\alpha_{Ex}^{out} \approx -1.9$. They are quite consistent with the input ones. The generated pomeron term has its intercept roughly equal to one $\alpha_P \approx 1$.

Next, we discuss the t-dependence of the elastic amplitudes which are believed to

be dominantly imaginary. These amplitudes calculated from Eqs (9) and (10) with the small t-approximation are found to be nearly exponential in t within the range $-0.15 < t < 0\ \mathrm{GeV}^2$. Therefore, in Table II and in Fig. 11 we quote only slope parameters b of the elastic differential cross sections (experimental data are taken from Ref. [16]). It turns out that the pomeron terms in pp and $p\bar{p}$ collisions have roughly equal slopes.

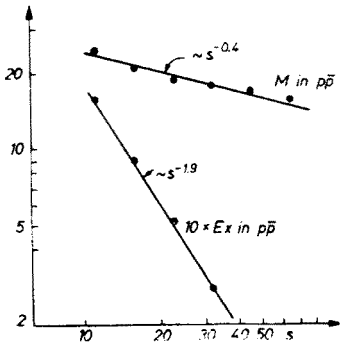

Fig. 10. The s-dependence of the meson and exotic exchange term in $p\bar{p}$ scattering

The slopes of the full $d\sigma_{el}/dt$ are lower but comparable to the ones expected from elastic scattering data. This discrepancy is much more serious for $p\bar{p}$ than for pp collisions. In our opinion, it arises from incorrect phase factors of baryon loops due to the assumed exchange degeneracy between $N_\alpha - N_\gamma$ trajectories[3].

We think that it also causes an exotic amplitude which is too large. In our model the ratio between the exotic and nonexotic cross sections at $p_{lab} = 5\ \mathrm{GeV}/c$ is $\sim 1:40$.

The total $p\bar{p}$ annihilation cross section is generated from graphs (i), (h), (t), (u), (w)

TABLE II

Slope parameters for different contributions to σ_{tot}

$s\ [\mathrm{GeV}^2]$		16	22	32	45
$\frac{d\sigma_{el}(pp)}{dt}$		5.24	6.82	8.34	9.6
$p\bar{p}$	P	6.02	6.77	7.5	8.1
	M	9.1	11.22	13.56	15.42
	Ex	10.5	12.	14.2	15.
$\frac{d\sigma_{el}(p\bar{p})}{dt}$		7.4	8.8	9.5	10.6

[3] It is well known that the elastic slope is very sensitive to the phase and spin dependence of the multiparticle amplitude [17]. Spins of the produced resonances (clusters) are taken into account in the sense of semi-local duality.

and (z) of Fig. 4. At $s = 12\,\mathrm{GeV}^2$ we obtain $\sigma_{\mathrm{ann}} = 19.5$ mb as compared to the experimental value $\sigma_{\mathrm{ann}}^{\mathrm{exp}} = (25 \pm 5)$ mb [16]. However, our σ_{ann} calculated in the two loops approximation falls, with increasing energy, faster than extrapolated low energy experimental data (as expected in this approximation).

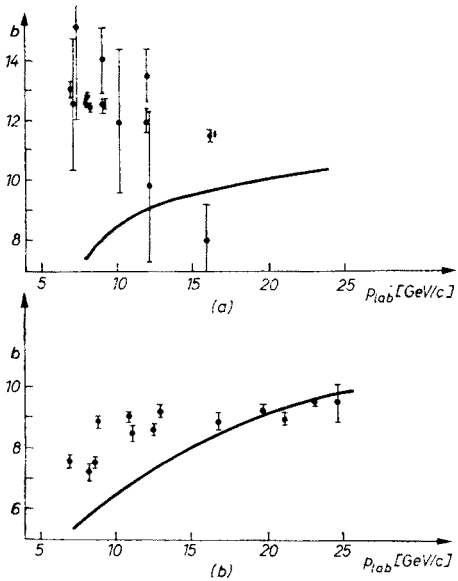

Fig. 11. Slope parameter of (a) the pp and (b) $\bar{p}p$ elastic differential cross sections

In our approach we have lost f-dominance of the pomeron. The breaking of this property is stronger in BB and $B\bar{B}$ than in MB and MM collisions due to the important role played by baryon exchange.

4. *Summary*

We have shown that the multi-Regge cluster model is able to explain the main features of the pp and $\bar{p}p$ elastic scattering if baryon exchanges are properly taken into account.

Our simplified model gives semi-quantitative agreement with experiment. We have obtained a crossing symmetric pomeron term. Annihilation channels give the piece which restores crossing symmetry in the low energy region. Thus our more explicit model supports the suggestion of Eylon and Harari [5]. However, contrary to the suggestion of Guła and Pennington, the diagram with two crossed meson loops is important even at low energy.

The output intercepts of the meson and exotic trajectories (in the elastic amplitude) are consistent with input values (in the multiparticle amplitude) but the output exotic coupling constant is too big.

The slope parameters of the $d\sigma_{\mathrm{el}}/dt$ are of the right order of magnitude. Numerical differences between obtained values and experimental data seem to be related to a breaking of the exchange degeneracy among meson and, especially, baryon trajectories.

I am grateful to S. Pokorski for suggesting this investigation and for many stimulating discussions. I also wish to thank Professor G. Białkowski and M. Święcki for reading the manuscript and many useful comments.

APPENDIX A

The analytic formula for the one loop diagram, after substitution of the triple-Regge vertices, phase factors and integration over t_1 and t_2, takes the following form (in small t approximation)

$$\operatorname{Im} T^{(1)}(t) = \frac{G}{2^8\pi^3 p_a \sqrt{s}} \int ds_1 ds_2 \frac{1}{a} v_1^{\alpha_{M_1}(0)} v_2^{\alpha_{M_2}(0)}$$

$$\times \left(\frac{v}{v_1 v_2}\right)^{2\alpha_x} (s_1')^{\alpha'_{M_1^t}} (s_2')^{\alpha'_{M_t^2}} \exp\left(2at_{1\min} + \frac{a^2-\pi^2 b\alpha'_x}{2a} \frac{k_1}{p_a} t\right) \tag{A1}$$

where $s_i = k_i^2$, $v_i = s_i - m_i^2$, $v = s - m_a^2 - m_b^2$, $a = \alpha'_x \log\left(\frac{s'}{s_1' s_2'} + R\right)$, $s_i' = v_i + c_i$,

$b = \begin{cases} 0 \text{ for crossed loop} \\ 1 \text{ for uncrossed loop} \end{cases}$, $c = \begin{cases} 1 & \text{for boson resonances} \\ 1.5 & \text{for fermion resonances} \end{cases}$, $p_b = \lambda^{1/2}(s, m_a^2, m_b^2)/2\sqrt{s}$,

$k_1 = \lambda^{1/2}(s, s_1, s_2)/2\sqrt{s}$, $\lambda(x, y, z)$ usual triangle function, $t_{1\min} = 2p_a k_1 - \lambda^*(s, s, m_a^2, s_1, m_b^2, s_2)/2s$, $\lambda^*(x, y, a, b, u, w) = xy + ab + uw - xb - ya - xw - yu - aw - bu$.

The kinematics is shown in Fig. 1. The $t_{1\min}$ is minimal momentum transfer. For a more detailed discussion of formula (A1) we refer to the original work [2].

For the two loop diagram we get

$$2 \operatorname{Im} T^{(2)}(t) = \frac{G}{2^{14}\pi^6} \int ds_1 ds_2 ds_3 ds_{12} \theta(s_{12} - r_1 \bar{s}) \theta(s_{23} - r_2 \bar{s})$$

$$\frac{k_1 k_3}{a_1 a_2 p_a^2 \sqrt{s s_{12}}\, k_3 q} v_1^{\alpha_{M_1} - 2\alpha_{x1}} v_2^{\alpha_{M_2} - \alpha_{x1} - \alpha_{x2}} v_3^{\alpha_{M_3} - 2\alpha_{x_2}}$$

$$v^{\alpha_{x1} + \alpha_{x2}} \left(\frac{v_{12}}{v_{23}}\right)^{\alpha_{x1} - \alpha_{x2}} (s_1' s_2' s_3')^{\alpha_{M'^t}} \exp\left[2a_1 t_{1\min} + 2a_2 t_{2\min}\right.$$

$$\left. + t\left(\frac{a_1^2 - \pi^2 \alpha'_{x_1} b_1}{2a_1 p_a} k_1 + \frac{a_2^2 - \pi^2 \alpha'_{x_2} b_2}{2a_2 p_a} k_3\right)\right] \tag{A2}$$

where $k_1 = \lambda^{1/2}(s, s_{23}, s_1)/2\sqrt{s}$, $k_3 = \lambda^{1/2}(s, s_{12}, s_3)/2\sqrt{s}$, $q = \lambda^{1/2}(s_{12}, s_1, s_2)/2\sqrt{s_{12}}$,

$a_i = \alpha'_{x_i} \log\left(\frac{s'_{i'i+1}}{s'_i s'_{i+1}} + R\right)$, $r_i = \begin{cases} 0 \text{ for crossed loop} \\ 1 \text{ for uncrossed loop,} \end{cases}$

$$s_{23} = \frac{1}{2s_{12}} [-\lambda^{1/2}(s, s_{12}, s_3)\lambda^{1/2}(s_{12}, s_1, s_2) - \lambda^*(s_{12}, s_{12}, s_2, s_3, s_1, s)].$$

Other symbols are defined as in Eq. (A1). The integrals over s_i are taken between the lowest resonance mass m_i^2 ($v_i = 0.$) and the cut-off value $\bar{s} = 6\ \mathrm{GeV}^2$ or the kinematical limit, whichever is smaller. To avoid double counting, there are θ-functions in Eq. (A2) which keep all loop energies $s_{i,i+1}$ for uncrossed loops greater than the cut-off value (configurations with $s_{i,i+1} < \bar{s}$ for uncrossed loop are already taken into account in a diagram with one loop less).

APPENDIX B

For the triple meson vertex (MMM) we take a simple parametrisation of Ref. [2]

$$[V(t, t_1, t_2)]^2 \approx \left(1 + R\frac{s_1 s_2}{s}\right)^{t_1 + t_2'}, \quad R = 1.5\ \mathrm{GeV}^{-2}, \tag{B1}$$

which is weakly dependent on t_1 (t_1') at small t_1 (t_1') and exponentially damped at large t_1 (t_1').

The relative strength of the meson couplings is fixed by the SU(3) symmetry with ideal mixing and by the exchange degeneracy. For the meson loops these couplings are (see Fig. 7a)

$$L_{\mathrm{MMM}} = \sum_{\mathrm{M_3 M_4}} g_{fff}^2 g_{\mathrm{M_4 \bar{M}_1 M_3}}(\tau_3 + e^{i\pi\alpha_3(t_1)}) g_{\mathrm{\bar{M}_4 M_2 \bar{M}_3}}(\tau_4 + e^{-i\pi\alpha_4(t_1')}) \tag{B2}$$

where $\lambda_{\bar{\mathrm{M}}_i} = c_i \lambda_{\mathrm{M}_i}^T$,

$$g_{\mathrm{M_1 M_2 M_3}} = \mathrm{Tr}\,(\lambda_{\mathrm{M_1}}\lambda_{\mathrm{M_2}}\lambda_{\mathrm{M_3}} + c_1 c_2 c_3 \lambda_{\mathrm{M_1}}\lambda_{\mathrm{M_2}}\lambda_{\mathrm{M_3}}). \tag{B3}$$

($g_{\mathrm{M_1 M_2 M_3}}$ denotes a triple meson coupling [14] and λ_i and c_i are the SU(3) λ-matrix and C-parity of the meson M_i, respectively). Parameter g_{fff} (triple f-coupling) is an overall normalisation and the sum in Eq. (6) is taken over the vector-tensor nonet trajectories.

Phase factors for crossed and uncrossed loops are 1 and $e^{i\pi(\alpha_3 - \alpha_4)}$, respectively. Therefore, the coefficient of 1 in formula (6) refers to crossed loops and the coefficient of $e^{i\pi(\alpha_3 - \alpha_4)}$ refers to uncrossed loops. Interference terms are cancelled out by EXD assumption. Baryon loops have the same phase factors and in case of only one baryon trajectory (nucleon N) the appropriate couplings are

$$L_{\mathrm{MNEx}} = 4 g_{\mathrm{NNEx}} g_{\mathrm{NNM}} \quad \text{(Fig. 7b)},$$

$$L_{\mathrm{ExNEx}} = 4(g_{\mathrm{NNEx}})^2 \quad \text{(Fig. 7c)}. \tag{B4}$$

The full coupling coefficient G for a given diagram is a product of the coefficients L and the couplings $\gamma_{\mathrm{M}}^{\mathrm{p}}$ of reggeons M to the external protons. We note that the f and ω exchange contributions to the pomeron term in BB and $\mathrm{B\bar{B}}$ scattering have the same sign. Therefore, there is no cancellation between diagrams as it was in Ref. [15] and the pomeron has only one component with $C = 1$.

REFERENCES

[1] Huan Lee, *Phys. Rev. Lett.* **30**, 719 (1973); G. Veneziano, *Phys. Lett.* **43B**, 413 (1973); Chan Hong-Mo, J. Paton, *Phys. Lett.* **46B**, 228 (1973).

[2] Chan Hong-Mo, J. Paton, Tsou Seung Tsun, *Nucl. Phys.* **B86**, 479 (1975).

[3] Chang Hong-Mo, J. Paton, Tsou Seung Tsun, S. W. Ng, *Nucl. Phys.* **B92**, 13 (1975).
[4] N. Sakai, Rutherford Lab. preprint RL-75-094.
[5] Y. Eylon, H. Harari, *Nucl. Phys.* **B80**, 349 (1974).
[6] P. G. O. Freund, R. J. Rivers, *Phys. Lett.* **29B**, 510 (1969).
[7] A. Guła, M. Pennington, Rutherford Lab. preprint RL-75-086.
[8] C. Baltay et al., State University of New York at Binghamton preprint (1975); D. Cohen, Columbia University preprint R. 922 (1974).
[9] D. Faiman, G. Goldhaber, Y. Zarmi, *Phys. Lett.* **43B**, 307 (1973); A. Pickering, Daresbury Lab. preprint DL/P 236 (1975).
[10] P. Hoyer, R. G. Roberts, D. P. Roy, *Nucl. Phys.* **B56**, 173 (1973); P. Hoyer, P. Estabrooks, A. Martin, Stony Brook preprint ITP-5B-74-3.
[11] P. Hoyer, R. G. Roberts, D. P. Roy, *Phys. Lett.* **44B**, 258 (1973).
[12] R. G. Roberts, *Acta Phys. Pol.* **B5**, 47 (1974).
[13] J. Dias de Deus, J. Uscherson, Rutherford Lab. preprint RL-75-042.
[14] J. Rosner, *Phys. Rev. Lett.* **22**, 689 (1969).
[15] C. Schmid, C. Sorensen, *Nucl. Phys.* **B96**, 209 (1975).
[16] E. Bracci et al., *Compilation of cross sections*; *p and* $\bar{p}$ *induced reactions*, CERN/HERA 73-1.
[17] L. Michejda, *Forts. Phys.* **16**, 707 (1968); Z. Ajduk, R. Stroynowski, *Phys. Lett.* **30B**, 179 (1969); S. Jadach, J. Turnau, *Acta Phys. Pol.* **B5**, 677 (1974) and references therein.